AMERICAN ACADEMY OF OPHTHALMOLOGY®

High-Resolution Characterization of Cone Photoreceptor Mosaic Alterations in Retinopathy of Prematurity Using Adaptive Optics Scanning Laser Ophthalmoscopy

Yaling Liu, PhD,[1,†] *Jiannan Tang, PhD,*[1,†] *Xinyu Zhao, PhD,*[1,†] *Yarou Hu, PhD,*[1] *Ziying Zhou, MS,*[1] *Zhen Yu, PhD,*[1] *Xiayuan Luo,*[1] *Mianying Zheng,*[1] *Guishuang Ying, PhD,*[2] *Guoming Zhang, PhD*[1]

Purpose: To characterize cone photoreceptor alterations using adaptive optics scanning laser ophthalmoscopy (AO-SLO) and explore their relationships with retinal structure, visual function, and ocular biometry in children with retinopathy of prematurity (ROP).

Design: Prospective observational case series.

Participants: A total of 313 eyes from 162 children were included, comprising full-term controls, preterm children without ROP, children with regressed ROP, and children with ROP treated with laser photocoagulation (LP), intravitreal anti-VEGF therapy, or combined therapy.

Methods: Participants underwent AO-SLO, swept-source OCT, best-corrected visual acuity testing, and ocular biometry. Cone density, dispersion, and regularity were evaluated across retinal regions. Between-group interpretation emphasized temporal cone metrics, and secondary exploratory analyses evaluated associations with retinal structural, visual, and biometric parameters.

Main Outcome Measures: Adaptive optics SLO–derived cone density, cone dispersion, and cone regularity across retinal regions, with temporal cone metrics considered the main region of interest.

Results: Among the clinically defined ROP subgroups, overall group differences in cone metrics were identified predominantly in the temporal region after multivariable adjustment ($P < 0.05$). In Bonferroni-adjusted pairwise comparisons, the LP + intravitreal injection clinical-background group showed lower temporal cone regularity than preterm children without ROP (94.5% vs. 96.4%; adjusted mean difference, −1.92%; Bonferroni-adjusted P=0.001), whereas temporal cone density and dispersion showed similar directional but nonsignificant pairwise differences. Laser-treated eyes showed greater inner retinal thickness (IRT) in selected regions ($P \leq 0.006$). Temporal cone regularity showed a weak positive association with temporal IRT ($r = 0.10$, generalized estimating equation–derived P=0.046; Table S6), whereas broader correlations between AO-SLO parameters and OCT measurements were generally limited.

Conclusions: Adaptive optics SLO identified selective temporal cone photoreceptor mosaic alterations in children with ROP, most consistently reflected by reduced temporal cone regularity, with directional differences in cone density and dispersion. These findings extend prior AO observations in ROP to a larger pediatric cohort and support AO-SLO as a complementary modality for evaluating cone spatial organization in ROP survivors.

Financial Disclosure(s): The author has no/the authors have no proprietary or commercial interest in any materials discussed in this article. *Ophthalmology Science 2026;6:101412* *© 2026 American Academy of Ophthalmology, Inc. Published by Elsevier Inc. This is an open access article under the CC BY-NC-ND license (http://creativecommons.org/licenses/by-nc-nd/4.0/).*

Supplemental material available at www.ophthalmologyscience.org.

Retinopathy of prematurity (ROP), a disorder of abnormal retinal vascular development in preterm infants, remains an important cause of potentially avoidable childhood visual impairment worldwide.[1,2] Retinopathy of prematurity affects approximately 30%–50% of very low birth weight infants globally, and timely management is critical to prevent severe visual impairment.[1] Beyond vascular abnormalities, increasing evidence suggests that ROP is also associated with disrupted retinal neurodevelopment, which may contribute to long-term alterations in photoreceptor organization and visual function.[3] Current treatment options for ROP include laser photocoagulation (LP) to ablate the peripheral avascular retina to prevent neovascularization and intravitreal anti-VEGF injections (intravitreal injection [IVI]) to suppress neovascular activity.[4] Although these interventions are effective in

© 2026 American Academy of Ophthalmology, Inc
Published by Elsevier Inc. This is an open access article under the CC BY-NC-ND license (http://creativecommons.org/licenses/by-nc-nd/4.0/).
http://doi.org/10.1016/j.xops.2026.101412
ISSN 2666-9145/26

controlling disease progression, the long-term effects of ROP and its associated retinal developmental alterations on photoreceptor microstructure remain incompletely understood.

Previous imaging studies in ROP have largely relied on OCT to assess retinal abnormalities, including alterations in inner and outer retinal thickness (ORT).[5–7] Although OCT provides valuable tissue-level structural information, it does not directly resolve the cone mosaic or quantify cone spatial organization, including density, dispersion, and regularity.[8] Adaptive optics (AO) imaging technology, capable of compensating for ocular aberrations, has emerged as a noninvasive tool for high-resolution retinal imaging.[9] Adaptive optics scanning laser ophthalmoscopy (AO-SLO), a specific application of AO imaging, has been used to visualize and quantify cone photoreceptor abnormalities in retinal diseases, including retinitis pigmentosa,[10] central serous chorioretinopathy,[11] laser-induced retinopathy,[12] and age-related macular degeneration.[13] Previous AO studies in eyes with a history of ROP have demonstrated extrafoveal cone density and packing geometry alterations, including the study by Ramamirtham et al[14] using AO-SLO and OCT.[3] However, these studies were limited by relatively small sample sizes and primarily focused on cone density or packing geometry at selected retinal eccentricities. A broader characterization of cone spatial organization, incorporating cone density, dispersion, and regularity across different ROP clinical backgrounds, remains insufficiently defined. In addition, most OCT-based studies in ROP survivors have focused on retinal thickness and general anatomical features, whereas the relationships between AO-SLO–derived cone mosaic alterations and broader ocular structural, functional, and biometric parameters remain incompletely characterized.

A comprehensive evaluation of cone photoreceptor mosaic alterations across a broad spectrum of ROP severity and clinical treatment backgrounds may provide important insights into long-term macular and photoreceptor phenotypes in ROP survivors.[15] This study aimed to use high-resolution AO-SLO imaging to characterize cone photoreceptor density, dispersion, and regularity in children across a broad spectrum of ROP conditions, including preterm children without ROP, regressed ROP (R-ROP), and ROP treated with LP and/or anti-VEGF therapy. We further explored the relationships between cone metrics and retinal structural, visual, and biometric parameters obtained from swept-source OCT (SS-OCT), best-corrected visual acuity (BCVA), and ocular biometry. By integrating AO-SLO with multimodal retinal assessment in a large pediatric cohort, this study sought to define AO-SLO–based cone mosaic alterations in ROP survivors and provide a foundation for future longitudinal imaging studies.

Methods

This cohort study conducted at Shenzhen Eye Hospital was approved by the Institutional Review Board of Shenzhen Eye Hospital (Shenzhen, China; approval number: 20191206-01) and was conducted in accordance with the tenets of the Declaration of Helsinki. Written informed consent was obtained from the legal guardians of each participating child.

Participants

The study enrolled a total of 162 participants (313 eyes) from June 2024 to April 2026. All participants underwent multimodal ophthalmic examinations, including BCVA testing, ocular biometry, SS-OCT, and AO-SLO imaging. Because quantitative analyses depended on cooperation, fixation stability, image quality, and modality-specific acquisition quality, the number of eyes included in each analysis varied slightly and is reported in the corresponding tables.

Participants were grouped into 6 groups based on their ROP status and treatment modality: normal full-term control (normal control group, $n = 31$), preterm without ROP (P-noROP group, $n = 25$), R-ROP (R-ROP group, $n = 18$), ROP treated with LP (LP group, $n = 52$), ROP treated with IVI (IVI group, $n = 20$), and ROP treated with a combination of LP and IVI (LP + IVI group, $n = 16$). For the LP + IVI group, most infants were treated with IVI first, followed by LP if the initial treatment was ineffective; in other cases, LP was performed first, followed by IVI when needed. The inclusion criteria were based on clinical history and fundus findings. The R-ROP group included preterm children with a history of ROP that regressed without treatment. Because ROP zone and stage describe active disease severity and may change during the disease course, a single zone or stage was not assigned to spontaneously R-ROP eyes after stabilization. For treated ROP eyes, zone and stage were recorded according to the clinical findings at the time treatment was indicated. To maintain the integrity of image quality and ensure accurate interpretation of results, individuals were considered ineligible for the study if their affected eyes had any of the following: 1) history of prior eye surgery or ocular injuries: for ROP groups, any prior vitrectomy or retinal surgery (except LP or IVI), while for the normal control and P-noROP groups, any history of eye surgery or ocular injury; 2) presence of other ocular conditions, including cataract, retinal tears, inherited retinal disorders, or retinal detachment; 3) age outside the range of 6-16 years; 4) inability to cooperate with imaging or maintain fixation sufficiently for reliable image acquisition; and 5) myopia greater than −6.00 diopters (D). Reduced BCVA in an individual eye was not used as an absolute eye-level exclusion criterion if the participant was able to follow the internal fixation target and analyzable images could be obtained.

All participants underwent comprehensive ophthalmologic assessments for the retinal structure and function. Best-corrected visual acuity was measured monocularly in children using a standard 5-m decimal acuity chart (1.0 at 5 m); all tests were performed by the same experienced optometrist with the child's best refractive correction in place, and BCVA values were converted to logarithm of the minimum angle of resolution for analysis. Refractometry was performed using an autorefractor (KR-8800, Topcon) under cycloplegia with 0.5% compound tropicamide eyedrops; biometric measures were obtained with the IOLMaster (Carl Zeiss Meditec) for axial length (AL), anterior chamber depth, central corneal thickness, and lens thickness measurement; SS-OCT (TowardPi Medical Technology) for retinal thickness, and AO-SLO (Mona II, Robotrak Technologies) for cone photoreceptors.

AO-SLO System: Cone Photoreceptor Analysis

Adaptive optics images were acquired using a commercially available AO-SLO system (Mona II, Robotrak Technologies). The system offers 3 imaging modes, providing different fields of view

of 5 × 5° (approximately 1500 × 1500 μm), 2.4 × 2.4° (approximately 700 × 700 μm), and 1.2 × 1.2° (approximately 350 × 350 μm). After dilation of the pupil with tropicamide, participants were instructed to fixate on a green target controlled by the operator to facilitate image capture at 3° retinal eccentricity using the 2.4 × 2.4° mode. Adaptive optics SLO image scaling and cone-density outputs were based on the device software's nominal conversion of the angular field of view to retinal dimensions, rather than individualized AL-based ocular magnification correction. A schematic illustration of the AO-SLO regional layout is provided in Figure S1.

For each eye, AO-SLO imaging was attempted at the predefined retinal locations, and 2 to 5 image acquisitions were obtained at each location when possible, depending on fixation stability and participant cooperation. For quantitative analysis, the best-quality image from each predefined retinal location was selected before cone segmentation and metric export. Image selection was based on image focus, signal strength, motion artifact, fixation stability, completeness of cone mosaic visualization within the region of interest, and reliability of automated cone segmentation. Images were excluded from quantitative cone mosaic analysis if they showed poor focus or low signal, substantial motion artifact, unstable fixation, incomplete visualization of the cone mosaic within the region of interest, or unreliable automated cone segmentation. Cone metrics were generated using the Mona II software after automated cone segmentation, and segmentation outputs were reviewed for reliability before inclusion in the final analysis. Because the system did not provide a single validated numeric image-quality score for exclusion, final image inclusion was based on these predefined image-quality and segmentation-reliability criteria. The system is equipped with an artificial intelligence–based algorithm that facilitates automatic segmentation of cone photoreceptors and provides quantitative measures of cone morphology, including density, dispersion, and regularity.[16] Cone density was defined as the number of cones per square millimeter. Cone dispersion was exported by the Mona II software as a percentage-based metric reflecting the spatial dispersion of the cone mosaic, with higher values indicating greater variability in local cone spacing. Cone regularity was exported as a percentage-based metric reflecting the uniformity of cone arrangement, with values closer to 100% indicating a more regular mosaic.[17,18]

For a more comprehensive analysis of cone morphology, the 2.4 × 2.4° AO-SLO frame centered at the intended 3° retinal eccentricity was divided into 5 predefined regions of interest: central, nasal, temporal, superior, and inferior. In this context, the central region referred to the center of the AO-SLO analytical frame rather than the foveal center. The nasal, temporal, superior, and inferior regions were defined according to their relative location within the AO-SLO frame.

Swept-Source OCT: Retinal Thickness Measurements

OCT images were captured using SS-OCT (TowardPi Medical Technology) by an experienced examiner for quantitative analysis of retinal thickness. Retinal thickness measurements included the foveal region and the parafoveal ring surrounding the fovea with an inner diameter of 1 mm and an outer diameter of 3 mm. For AO-SLO–OCT correlation analyses, OCT measurements were paired with AO-SLO metrics according to the corresponding regional orientation, including nasal, temporal, superior, inferior, and central regions. This approach provided regional topographic correspondence rather than direct image-to-image registration between AO-SLO and OCT images, as illustrated in Figure S1. Measurements were conducted for multiple retinal layers, including inner retinal thickness (IRT), defined as the distance from the inner limiting membrane to the inner plexiform layer; ORT, defined as the distance from the inner plexiform layer to Bruch's membrane; and total retinal thickness, defined as the distance from the inner limiting membrane to Bruch's membrane.

Statistical Analyses

Continuous data were summarized using mean ± standard deviation, and categorical variables as counts and percentages. Group comparisons were performed using 1-way analysis of variance, chi-square tests, or generalized linear models with generalized estimating equations (GEEs), as appropriate, to account for intereye correlation. For model-based group comparisons, values are presented as estimated marginal means with standard errors of the mean, unless otherwise specified. For post hoc pairwise comparisons, Bonferroni correction was applied to adjust for multiple comparisons, and a corrected P value < 0.05 was considered statistically significant.

Adaptive optics SLO analyses included cone density, dispersion, and regularity measured across the retinal regions. For interpretation of between-group AO-SLO differences, the temporal region was treated as the main region of interest, whereas findings from the superior, inferior, nasal, and central regions were reported as supportive regional analyses. Multivariable models were adjusted for gestational age (GA), age at examination, sex, and AL, which were selected as clinically relevant covariates related to prematurity, ocular development, retinal image magnification, and AO-SLO measurement. Retinopathy of prematurity zone and stage were summarized descriptively but were not included in the primary 6-group models because these variables were not applicable to full-term controls or preterm children without ROP and were closely related to the clinical-background/treatment group definitions. Secondary exploratory analyses evaluated associations between AO-SLO metrics and retinal structural, visual, and ocular biometric parameters. Pearson correlation coefficients were calculated directly from paired eye-level data to describe the strength and direction of linear associations. Corresponding P values were obtained from GEE models to account for intereye correlation within participants. The reported correlation coefficients therefore represent Pearson r values rather than standardized regression coefficients from the GEE models. For AO-SLO–OCT correlation analyses, only eyes with paired analyzable AO-SLO and SS-OCT measurements from the same eye were included. Given the exploratory nature of these analyses and multiple comparisons, correlation findings were interpreted cautiously. All statistical analyses were conducted using SPSS software (version 23.0). All tests were 2-sided, and $P < 0.05$ was considered statistically significant unless otherwise specified.

Results

Participants' Demographics and Clinical Characteristics

The study included 162 participants (313 eyes) in 6 groups: normal full-term control (31 participants, 57 eyes), P-noROP (25 participants, 50 eyes), R-ROP (18 participants, 34 eyes), LP (52 participants, 101 eyes), IVI (20 participants, 40 eyes), and LP + IVI (16 participants, 31 eyes). The detailed patient recruitment flowchart is presented in Figure 1. Baseline demographic information, including ROP zone, ROP stage, GA, birth weight, age at examination, and sex, is provided in Table 1.

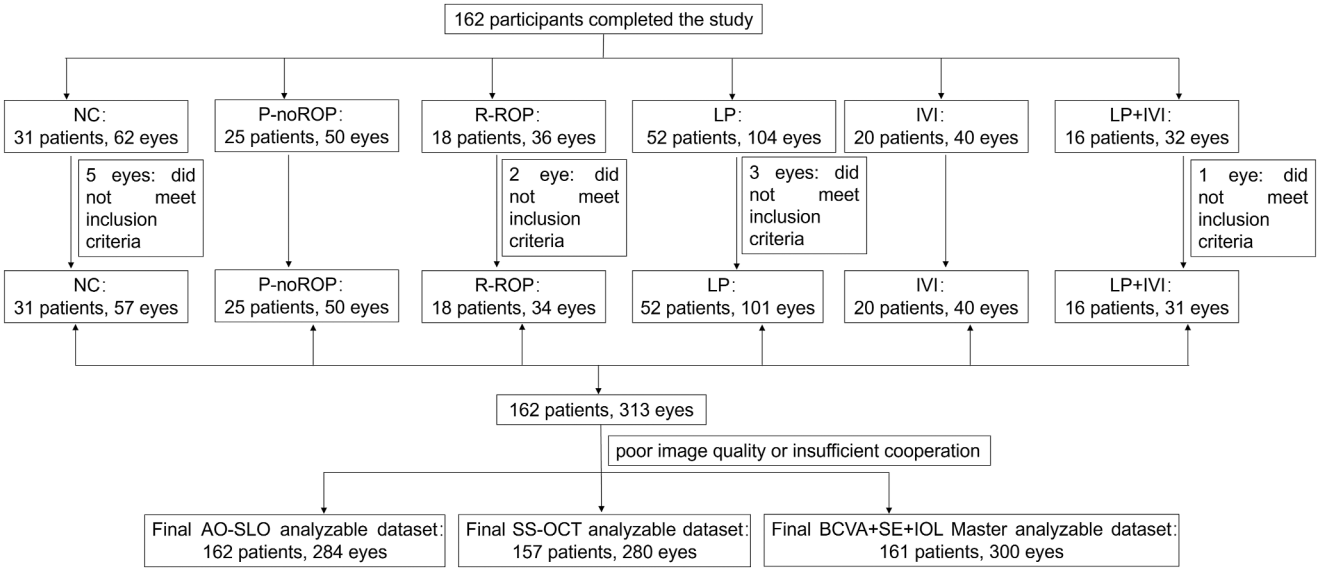


Figure 1. Participant enrollment and modality-specific analyzable data sets. A total of 162 participants contributed 313 eyes after application of eye-level eligibility criteria. Because analyzable data depended on participant cooperation, fixation stability, image quality, and modality-specific acquisition quality, the number of eyes included in each analysis varied slightly. The final analyzable data sets included 284 eyes for AO-SLO, 280 eyes for SS-OCT, and 300 eyes for BCVA, SE, and IOL Master measurements. Eyes not included in a modality-specific data set had insufficient image quality or inadequate cooperation for reliable quantitative analysis. AO-SLO = adaptive optics scanning laser ophthalmoscopy; SS-OCT = swept-source OCT; NC = normal full-term control; P-noROP = preterm without ROP; R-ROP = regressed ROP; LP = laser photocoagulation; IVI = intravitreal injection; LP + IVI = ROP treated with a combination of LP and IVI (LP + IVI); BCVA = best-corrected visual acuity; SE = spherical equivalent.

Significant differences in GA and birth weight were observed among the 6 groups (both $P < 0.001$), primarily driven by comparisons between full-term controls and preterm participants (Fig S2). Among the treated ROP groups, the recorded ROP zone and stage did not differ significantly across the LP, IVI, and LP + IVI groups (Table 1).

AO-SLO Characterization of Cone Photoreceptor Mosaic Alterations

All 162 participants underwent attempted AO-SLO imaging. Among the 313 examined eyes, 284 eyes met the image-quality criteria and were included in the final

Table 1. Demographics Parameters in Normal Full-Term Control, Premature without ROP, Regressive ROP, and Treatment Groups (LP, IVI, and LP + IVI)

	Normal Control	Premature without ROP	Regressive ROP	LP	IVI	LP + IVI	*P* Value
No. of patients	31	25	18	52	20	16	
No. of eyes	57	50	34	101	40	31	
Sex (M/F)	15/16	10/15	10/8	24/28	10/10	11/5	0.58
ROP zone, eyes (%)							0.18
II	NA	NA	NA	86 (85.1%)	36 (90%)	23 (74.2%)	
III	NA	NA	NA	15 (14.9%)	4 (10%)	8 (25.8%)	
ROP stage, eyes (%)							0.99
2	NA	NA	NA	19 (18.8%)	8 (20%)	6 (19.4%)	
3	NA	NA	NA	82 (81.2%)	32 (80%)	25 (80.6%)	
GA (w), mean ± SD	38.87 ± 2.21	30.57 ± 3.01	28.12 ± 2.55	29.35 ± 3.03	28.3 ± 3.30	27.91 ± 2.57	**<0.001**
BW (kg), mean ± SD	3.28 ± 0.99	1.45 ± 0.44	1.14 ± 0.48	1.28 ± 0.53	1.18 ± 0.41	1.07 ± 0.39	**<0.001**
Age (y), mean ± SD	10.51 ± 2.83	9.70 ± 3.85	8.07 ± 2.06	8.84 ± 2.26	9.31 ± 2.13	8.54 ± 2.01	**0.025**

Using chi-square test for comparison of proportions and 1-way analysis of variance for comparison of means. Retinopathy of prematurity zone and stage were reported for treated eyes according to the treatment records at the time treatment was indicated. For the regressed ROP group, eyes had a history of ROP that regressed without treatment; because ROP zone and stage may change during the active disease course and were not assigned after spontaneous regression, a single final zone or stage was not reported for this group. Plus disease status was not consistently available in the historical records and therefore was not reported as a separate variable. Bold values indicate statistical significance ($P < 0.05$).
LP = laser photocoagulation; IVI = intravitreal injection; LP + IVI = ROP treated with a combination of LP and IVI (LP + IVI); NA = not applicable; ROP = retinopathy of prematurity; BW = birth weight; SD = standard deviation; GA = gestational age.

Table 2. Temporal AO-SLO Parameters in Normal Full-Term Control, Premature without ROP, Regressive ROP, and Treatment Groups (LP, IVI, and LP + IVI)

	Estimated Marginal Mean ± SEM						
	Normal Control	*Premature without ROP*	*Regressive ROP*	*LP*	**IVI**	**LP + IVI**	**P Value**
Temporal cone density (cones/mm^2)							
Unadjusted	24 161.99 ± 1090.71	23 145.87 ± 629.38	26 563.51 ± 995.10	24 528.96 ± 812.74	24 871.83 ± 1401.90	28 093.54 ± 1697.14	**0.019**
Adjusted 1	24 299.49 ± 1119.8	23 181.09 ± 663.24	26 540.72 ± 987.83	24 409.94 ± 812.16	24 964.63 ± 1399.74	28 101.60 ± 1709.14	**0.02**
Adjusted 2	24 508.78 ± 1402.67	23 117.98 ± 657.97	26 447.79 ± 1029.12	24 411.71 ± 873.53	24 919.63 ± 1452.74	28 011.57 ± 1730.86	**0.026**
Adjusted 3	23 616.98 ± 1099.63	23 135.49 ± 705.04	26 514.17 ± 1006.89	23 738.48 ± 774.77	24 633.06 ± 1276.57	26 303.36 ± 1084.44	**0.035**
Temporal cone dispersion (%)							
Unadjusted	19.63 ± 0.53	18.04 ± 0.56	19.69 ± 0.62	19.90 ± 0.49	19.81 ± 0.67	20.92 ± 0.82	**0.054**
Adjusted 1	19.58 ± 0.55	18.02 ± 0.58	19.61 ± 0.62	19.94 ± 0.40	19.78 ± 0.66	20.92 ± 0.83	**0.059**
Adjusted 2	19.26 ± 0.77	17.94 ± 0.60	19.56 ± 0.61	20.11 ± 0.40	19.89 ± 0.68	20.94 ± 0.82	**0.036**
Adjusted 3	19.25 ± 0.79	18.08 ± 0.61	19.75 ± 0.63	20.03 ± 0.38	20.03 ± 0.66	21.01 ± 0.80	**0.047**
Temporal cone regularity (%)							
Unadjusted	95.22 ± 0.31	96.34 ± 0.25	95.39 ± 0.35	95.09 ± 0.23	95.06 ± 0.30	94.56 ± 0.39	**<0.001**
Adjusted 1	95.29 ± 0.31	96.39 ± 0.26	95.35 ± 0.34	95.04 ± 0.22	95.09 ± 0.30	94.54 ± 0.40	**<0.001**
Adjusted 2	95.26 ± 0.46	96.45 ± 0.27	95.42 ± 0.35	94.98 ± 0.25	95.09 ± 0.31	94.59 ± 0.39	**<0.001**
Adjusted 3	95.61 ± 0.48	96.39 ± 0.28	95.34 ± 0.35	94.91 ± 0.24	95.01 ± 0.31	94.47 ± 0.39	**<0.001**

Generalized estimating equations were used for both unadjusted and adjusted analyses to account for intereye correlation. Post hoc pairwise comparisons were adjusted using the Bonferroni correction. Bonferroni-adjusted post hoc pairwise comparisons from the fully adjusted model are shown in Table S1. Bold values indicate statistical significance ($P < 0.05$).
AO-SLO = adaptive optics scanning laser ophthalmoscopy; SEM = standard error of the mean; LP = laser photocoagulation; IVI = intravitreal injection; LP + IVI = ROP treated with a combination of LP and IVI (LP + IVI); ROP = retinopathy of prematurity; Adjusted 1 = adjusted for age and sex; Adjusted 2 = adjusted for age, sex, and gestational age; Adjusted 3 = adjusted for age, sex, gestational age, and axial length.

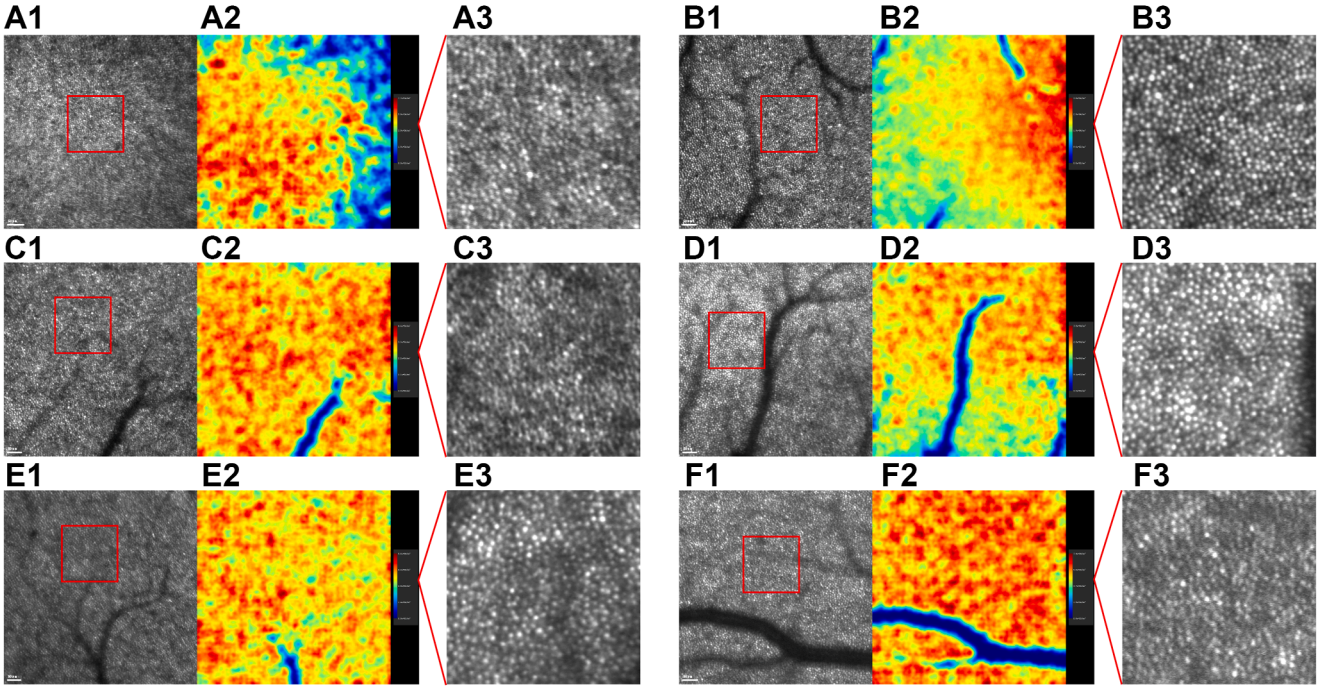


Figure 2. The temporal AO-SLO images across 6 groups. **A**-**F**, AO-SLO cone photoreceptor images, corresponding heatmaps, and magnified views of the temporal local region. Specifically: **A**. NC group (**A1**: AO-SLO images, A2: heatmap, and **A3**: magnified view of **A1**); **B**. P-noROP group; **C**. R-ROP group; **D**. LP group; **E**. IVI group; and **F**. LP + IVI group. AO-SLO = adaptive optics scanning laser ophthalmoscopy; NC = normal full-term control; P-noROP = preterm without ROP; R-ROP = regressed ROP; LP = laser photocoagulation; IVI = intravitreal injection; LP + IVI = ROP treated with a combination of LP and IVI (LP + IVI).

Table 3. Inner Ring of IRT Parameters from OCT in Normal Control, Premature without ROP, Regressive ROP, and Treatment Groups (LP, IVI, and LP + IVI)

	Estimated Marginal Mean ± SEM						
IRT Parameters (μm)	*Normal Control*	*Premature without ROP*	*Regressive ROP*	*LP*	*IVI*	*LP + IVI*	**P Value**
Macular fovea							
Unadjusted	78.04 ± 6.74	75.85 ± 1.87	90.03 ± 8.96	94.03 ± 4.78	85.47 ± 4.17	90.84 ± 5.85	**0.001**
Adjusted 1	71.96 ± 6.49	73.23 ± 3.37	94.18 ± 9.06	94.16 ± 4.32	85.19 ± 4.66	93.13 ± 5.98	**0.002**
Adjusted 2	77.85 ± 7.96	73.07 ± 3.31	93.22 ± 9.00	93.79 ± 4.30	83.92 ± 4.58	91.84 ± 6.03	**0.006**
Temporal region							
Unadjusted	113.48 ± 4.90	120.30 ± 2.24	126.67 ± 6.97	126.73 ± 1.82	111.25 ± 2.90	123.00 ± 3.98	**<0.001**
Adjusted 1	111.35 ± 5.09	120.86 ± 2.14	128.17 ± 7.18	126.76 ± 1.62	111.14 ± 3.09	123.84 ± 4.09	**<0.001**
Adjusted 2	109.93 ± 6.17	120.85 ± 2.11	128.44 ± 7.04	126.78 ± 1.66	111.60 ± 3.06	124.20 ± 4.06	**<0.001**
Superior region							
Unadjusted	123.22 ± 4.80	129.50 ± 1.79	135.64 ± 8.93	140.07 ± 3.43	123.47 ± 3.40	134.53 ± 5.35	**0.008**
Adjusted 1	118.51 ± 4.73	128.38 ± 3.24	138.65 ± 8.99	140.25 ± 3.05	123.31 ± 3.57	136.14 ± 5.68	**<0.001**
Adjusted 2	114.91 ± 7.59	128.57 ± 3.28	139.18 ± 9.00	140.60 ± 3.12	123.81 ± 3.53	136.85 ± 5.47	**0.002**
Nasal region							
Unadjusted	122.07 ± 6.23	130.20 ± 1.16	139.97 ± 9.54	147.30 ± 7.94	122.22 ± 3.56	130.84 ± 5.05	**0.03**
Adjusted 1	112.67 ± 7.60	127.92 ± 4.27	146.22 ± 9.43	147.56 ± 7.21	121.83 ± 4.52	134.24 ± 5.40	**0.03**
Adjusted 2	103.58 ± 10.78	127.85 ± 4.72	147.92 ± 9.60	147.71 ± 6.93	124.77 ± 5.17	136.49 ± 5.67	**0.02**
Inferior region							
Unadjusted	122.67 ± 6.56	128.28 ± 2.29	137.79 ± 8.58	141.83 ± 4.03	118.92 ± 4.22	138.28 ± 7.65	**0.002**
Adjusted 1	117.58 ± 7.11	127.19 ± 3.11	140.97 ± 8.77	142.04 ± 3.61	118.76 ± 4.40	139.96 ± 7.86	**<0.001**
Adjusted 2	109.26 ± 8.15	127.35 ± 3.16	142.37 ± 8.68	142.48 ± 3.63	120.76 ± 4.44	141.83 ± 7.91	**<0.001**

Generalized estimating equations were used for both unadjusted and adjusted analyses to account for intereye correlation. Post hoc pairwise comparisons were adjusted using the Bonferroni correction. Bold values indicate statistical significance ($P < 0.05$).
IRT = inner retinal thickness; SEM = standard error of the mean; LP = laser photocoagulation; IVI = intravitreal injection; LP + IVI = ROP treated with a combination of LP and IVI (LP + IVI); ROP = retinopathy of prematurity; Adjusted 1 = adjusted for age and sex; Adjusted 2 = adjusted for age, sex, gestational age.

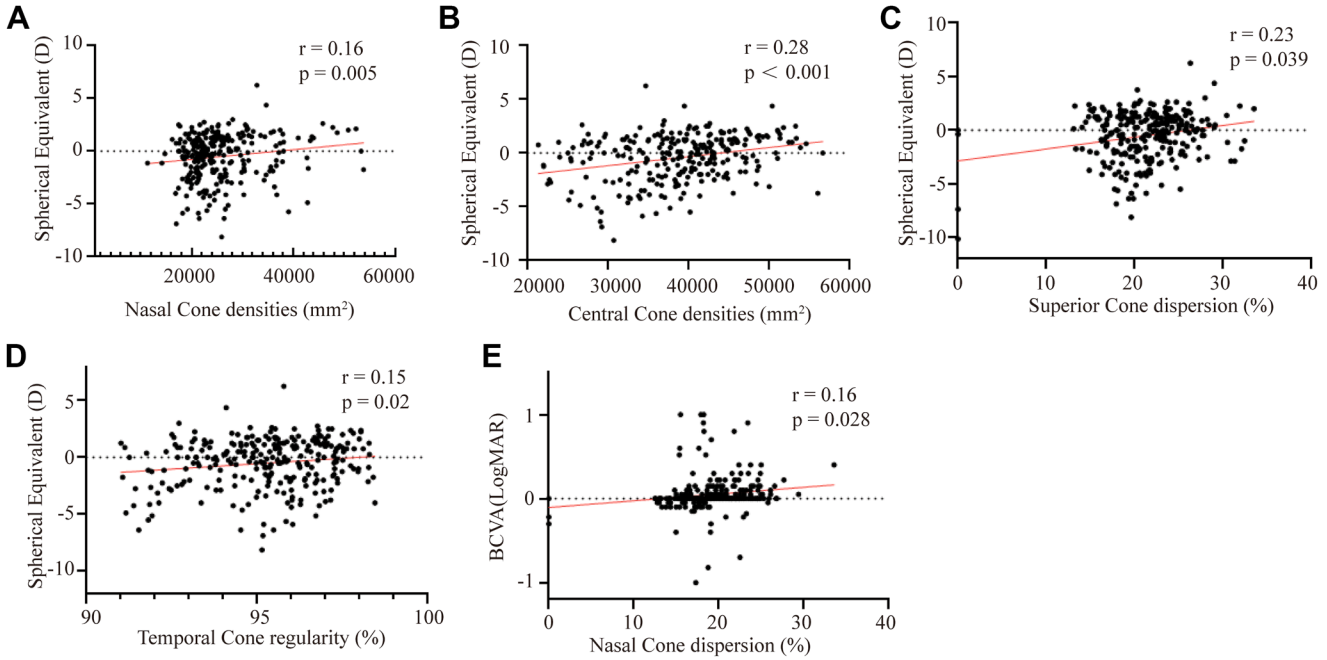


Figure 3. Correlations between AO-SLO cone morphology parameters and visual function or refractive measurements. **A**. Correlation between nasal cone densities and SE. **B**. Correlation between central cone dispersion and SE. **C**. Correlation between superior cone dispersion and SE. **D**. Correlation between temporal cone regularity and SE. **E**. Correlation between nasal cone dispersion and BCVA. Pearson correlation analysis was performed, and generalized estimating equations were used to account for intereye correlation. Correlation findings were interpreted cautiously in the context of multiple comparisons. Associations with BCVA were exploratory and limited. BCVA = best-corrected visual acuity; AO-SLO = adaptive optics scanning laser ophthalmoscopy; LogMAR = logarithm of the minimum angle of resolution; SE = spherical equivalent.

quantitative AO-SLO analysis. The remaining 29 eyes were not included in AO-SLO quantitative analysis because of insufficient image quality, unstable fixation or motion artifacts, incomplete cone mosaic visualization, or unreliable automated segmentation (Figure 1). Adaptive optics SLO measures were compared among the 6 groups using unadjusted and multivariable-adjusted models. Overall group differences in temporal cone density, dispersion, and regularity were observed in the fully adjusted models ($P < 0.05$, Table 2). Bonferroni-adjusted post hoc pairwise comparisons from the fully adjusted model are shown in Table S1. Compared with the P-noROP group, the LP + IVI group had significantly lower temporal cone regularity (94.47% vs. 96.39%; adjusted mean difference, −1.92%; 95% confidence interval, −3.34 to −0.50; Bonferroni-adjusted P=0.001). Temporal cone density (26 303 vs. 23 135 cones/mm^2; Bonferroni-adjusted P=0.23) and dispersion (21.01% vs. 18.08%; Bonferroni-adjusted P=0.06) showed the same directional pattern but did not remain statistically significant after Bonferroni adjustment. In contrast, no consistent between-group differences were identified in most nontemporal retinal regions (Table S2).

Representative AO-SLO images demonstrated alterations in cone spatial organization across ROP groups, particularly in eyes in the LP + IVI clinical-background group, characterized by increased cone dispersion and reduced regularity (Fig 2).

Secondary Structural and Functional Ocular Findings

For SS-OCT measurements, no significant differences in ORT were identified among the 6 groups across retinal regions (Table S3). In contrast, significant differences in IRT were observed in multiple retinal regions after multivariable adjustment ($P \leq 0.03$, Table 3). After multivariable adjustment, the LP group generally demonstrated greater IRT measurements across multiple retinal regions, whereas thinner IRT values were observed in full-term controls or preterm children without ROP, depending on retinal location.

Total retinal thickness differed significantly only in the central macular region after multivariable adjustment (P = 0.02, Table S4). No statistically significant differences in spherical equivalent were identified among the 6 groups (Table S5). Significant differences were also observed for BCVA and several ocular biometric parameters, including AL, anterior chamber depth, central corneal thickness, and lens thickness (all $P \leq 0.002$, Table S5).

Exploratory Associations between AO-SLO Metrics and Ocular Parameters

Exploratory correlation analyses were performed to evaluate associations between AO-SLO cone metrics and structural, functional, and biometric parameters. Adaptive

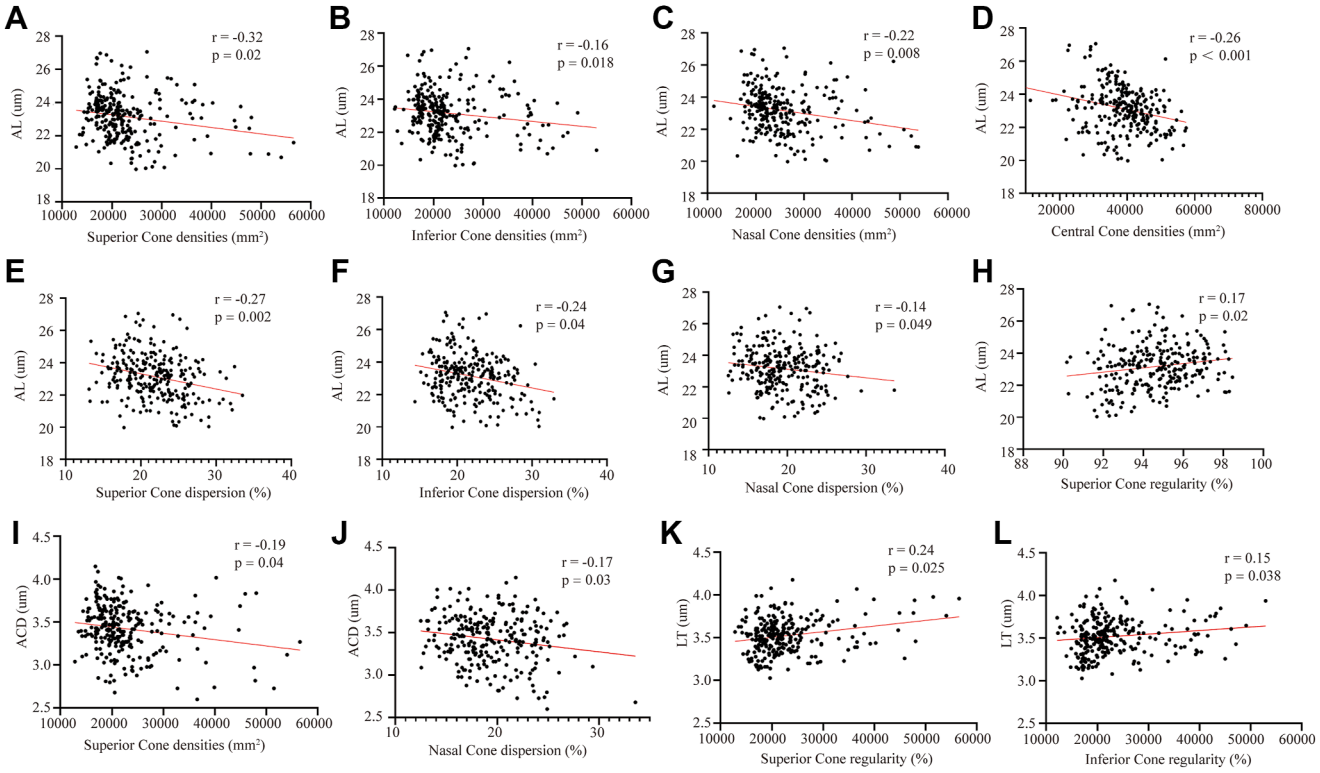


Figure 4. Correlations between cone morphology parameters from AO-SLO and biometric measurements (AL and ACD) from IOL Master. **A**. Correlation between superior cone densities and AL. **B**. Correlation between inferior cone densities and AL. **C**. Correlation between nasal cone densities and AL. **D**. Correlation between central cone densities and AL. **E**. Correlation between superior cone dispersion and AL. **F**. Correlation between inferior cone dispersion and AL. **G**. Correlation between nasal cone dispersion and AL. **H**. Correlation between superior cone regularity and AL. **I**. Correlation between superior cone densities and ACD. **J**. Correlation between nasal cone dispersion and ACD. **K**. Correlation between superior cone regularity and LT. **L**. Correlation between inferior cone regularity and LT. Pearson correlation analysis was performed, and generalized estimating equations were used to account for intereye correlation. Correlation findings were interpreted cautiously in the context of multiple comparisons. AO-SLO = adaptive optics scanning laser ophthalmoscopy; AL = axial length; ACD = anterior chamber depth; LT = lens thickness.

optics SLO−OCT correlations were based only on eyes with paired analyzable AO-SLO and SS-OCT measurements from the same eye; the corresponding paired-eye counts are shown in Table S6. Temporal cone regularity showed a weak positive association with temporal IRT ($r = 0.10$, $P = 0.046$; Table S6), but it was not significantly associated with BCVA ($r = -0.05$, $P = 0.40$; Table S7). Overall, associations between AO-SLO metrics and BCVA were limited and exploratory (Table S7, Fig 3), and broader correlations between AO-SLO parameters and OCT measurements were generally limited.

Among ocular biometric parameters, AL demonstrated modest associations with several cone morphology metrics (Table S8, Fig 4). Other biometric parameters, including anterior chamber depth and lens thickness, demonstrated only weak or inconsistent relationships with cone morphology measurements.

Discussion

Retinopathy of prematurity is increasingly recognized not only as a disorder of abnormal retinal vascularization, but also as a condition associated with altered retinal neurodevelopment and long-term changes in visual system maturation.[19,20] In this study, we used high-resolution AO-SLO to characterize cone photoreceptor morphology across a broad spectrum of ROP conditions and treatment backgrounds in a large pediatric cohort. The principal finding was the presence of selective temporal cone photoreceptor mosaic alterations in children with ROP. In the temporal retina, the most robust Bonferroni-adjusted pairwise finding was lower cone regularity in the LP + IVI clinical-background group compared with preterm children without ROP. Temporal cone density and dispersion showed similar directional differences in the fully adjusted model, but these pairwise comparisons did not remain statistically significant after Bonferroni adjustment. In contrast, most nontemporal retinal regions showed no consistent between-group differences. Together, these findings define a regionally selective cone spatial organization phenotype in ROP survivors rather than a diffuse photoreceptor abnormality.

These findings highlight the importance of evaluating cone spatial organization beyond density alone. Although eyes in the LP + IVI clinical-background group showed

numerically higher temporal cone density and dispersion, the most robust Bonferroni-adjusted pairwise finding was reduced temporal cone regularity. This pattern supports altered cone spatial organization rather than uniformly preserved photoreceptor architecture. The cone mosaic is defined not only by the number of cones in a given area, but also by the spatial relationship among neighboring cones, the uniformity of cone packing, and the regularity of the cellular arrangement.[3,15] This interpretation is consistent with the developmental biology of the human fovea, in which postnatal maturation involves coordinated redistribution of inner retinal elements, cone migration, progressive cone packing, and changes in cone spacing.[21] Therefore, a localized increase in cone density may reflect altered developmental packing or regional differences in retinal expansion, rather than a straightforward marker of normal photoreceptor organization.

The broader AO-SLO literature also supports this interpretation. In healthy eyes, cone density and spacing vary substantially by retinal eccentricity and region, emphasizing the need to interpret cone density in the context of retinal location and mosaic geometry rather than as an isolated metric.[15] In resolved central serous chorioretinopathy, AO-SLO identified abnormal cone mosaic patterns and patchy dark regions, and these microstructural changes were related to visual and OCT findings, but the relationship between cone density and conventional imaging was not always linear.[11] Similarly, in epiretinal membrane, AO-SLO revealed microfold-like abnormalities and disrupted cone arrangement, showing that photoreceptor mosaic organization may be abnormal even when conventional OCT or visual acuity does not fully explain the phenotype.[8] These studies are relevant to the present work because they demonstrate that cone spatial organization can provide information beyond cone counts alone. Thus, the temporal phenotype observed in our ROP cohort is best understood as cone mosaic alterations, characterized by altered spatial organization, rather than simple cone loss or preservation.

The temporal localization of cone mosaic alterations may have developmental relevance. Human foveal and parafoveal maturation continues beyond birth, and premature birth may interrupt this highly coordinated process.[21] Previous OCT studies in children with ROP have demonstrated persistent differences in foveal architecture, retinal layer thickness, and inner retinal configuration, supporting the concept that ROP affects retinal development beyond the vascular compartment.[6,8,22,23] In our cohort, AO-SLO abnormalities were concentrated in the temporal retina, whereas most other regions showed no consistent between-group differences. This regional pattern suggests that temporal cone mosaic alterations may represent a localized developmental vulnerability in ROP survivors. It also provides a plausible explanation for why AO-SLO detected microstructural abnormalities that were not uniformly reflected by global OCT thickness or BCVA.

The distinct temporal cone mosaic phenotype observed in LP + IVI clinical-background group should be interpreted within the broader clinical context of ROP disease activity, recurrence, and cumulative treatment exposure. Eyes requiring both LP and intravitreal anti-VEGF therapy often represent more complex clinical courses, including persistent disease activity, recurrence, greater ischemic burden, or cumulative treatment exposure. Because ROP zone and stage were not applicable to all comparison groups and were closely linked to treatment-background classification, they were not included in the primary 6-group multivariable models. Among treated ROP groups, recorded ROP stage and zone did not differ significantly, which partially reduces concern regarding baseline severity differences. Nevertheless, stage and zone alone do not fully capture disease activity, posterior vascular behavior, timing of treatment, recurrence pattern, number of injections, or cumulative ischemic exposure. Therefore, residual confounding by ROP severity cannot be fully excluded.

Experimental evidence that VEGF signaling contributes to retinal neuronal maintenance and cone photoreceptor function provides a useful biological context for these findings.[24–26] However, these data are derived mainly from preclinical models and cannot be directly extrapolated to long-term clinical outcomes in children treated with intravitreal anti-VEGF therapy for ROP. In the present study, the IVI-only group did not demonstrate the same temporal cone phenotype as the LP + IVI group. This observation argues against a simple explanation that anti-VEGF exposure alone accounts for the observed cone mosaic alterations. A more biologically plausible interpretation is that the observed phenotype reflects the combined influence of prematurity, altered retinal development, disease activity, ischemic burden, and cumulative treatment exposure. Accordingly, our findings are best viewed as characterization of cone mosaic alterations across clinically defined ROP backgrounds rather than as a comparison of causal treatment effects.

The SS-OCT findings provide complementary structural context. We observed significant differences in IRT, whereas ORT did not differ significantly among groups. The LP group generally demonstrated greater IRT across multiple regions, which may reflect persistent inner retinal developmental alteration or incomplete inner retinal displacement associated with ROP history and treatment background.[6–8,27–31] However, the weak positive association between temporal IRT and temporal cone regularity should not be interpreted as evidence that greater IRT is associated with reduced cone regularity. Rather, the limited and directionally modest AO-SLO–OCT correlations suggest that cone mosaic organization and retinal layer thickness capture related but distinct aspects of retinal development. The absence of consistent ORT differences is also informative. It suggests that AO-SLO may reveal cone mosaic alterations that are not fully captured by retinal layer thickness measurements. OCT provides tissue-level cross-sectional information, whereas AO-SLO enables high-resolution visualization of the cone mosaic. Therefore, AO-SLO and OCT should be considered complementary modalities for assessing retinal developmental alterations in ROP, rather than redundant measurements of the same structural feature.

Associations between AO-SLO metrics and BCVA were limited in the present study. Although temporal cone regularity showed a weak association with temporal IRT, it was not significantly associated with BCVA. This finding should therefore be interpreted as a localized structure−structure association rather than evidence of a direct structure−function relationship. The limited BCVA association does not necessarily reduce the biological relevance of AO-SLO findings. Best-corrected visual acuity is a relatively global measure of central visual performance and may remain preserved despite localized photoreceptor mosaic abnormalities. Similarly, OCT thickness measurements may remain relatively stable even when cellular-level cone packing geometry is altered. Previous AO-SLO studies in central serous chorioretinopathy, epiretinal membrane, and laser-induced retinopathy have shown that photoreceptor mosaic changes may not always parallel conventional functional measures, including visual acuity or retinal sensitivity.[8,11,12] In this sense, the limited correlations in the present study may reflect the subclinical nature of cone mosaic alterations in older, cooperative children with treated or R-ROP, rather than a lack of biological significance.

Ocular biometry may further influence the interpretation of AO-SLO metrics. In exploratory analyses, AL demonstrated modest associations with several cone morphology parameters. Prior AO imaging studies have shown that cone topography and apparent cone density are influenced by eye length, retinal magnification, and retinal stretching.[32] Children with ROP may also show distinctive refractive and biometric development after premature birth and treatment.[28,32−35] Therefore, AL is an important covariate when interpreting cone density and spatial metrics in pediatric ROP cohorts. However, because the correlations observed in this study were modest and exploratory, AL should be considered a potential modifier of AO-SLO measurements rather than a definitive explanation for the observed temporal cone phenotype.

This study has several strengths. First, to our knowledge, it represents one of the largest pediatric AO-SLO cohorts in ROP reported to date. Previous AO-SLO studies in ROP have generally included smaller samples and focused mainly on cone density or packing geometry at selected retinal eccentricities.[3,14] In contrast, the present study included 313 eyes from 162 children, with AO-SLO cone morphology successfully analyzed in 284 eyes, enabling evaluation of cone density, dispersion, and regularity across multiple retinal regions. Second, the integration of AO-SLO with SS-OCT, BCVA, and ocular biometric measurements enabled a multimodal assessment of retinal developmental alterations. Third, the use of multivariable-adjusted models and GEE allowed partial control for demographic, perinatal, biometric, and intereye correlation factors. These features support the robustness of the observed temporal cone mosaic alterations phenotype.

Several limitations should be acknowledged. First, the cross-sectional design precludes conclusions regarding the longitudinal trajectory of cone development. Second, although recorded ROP stage and zone were comparable among treatment groups and the models adjusted for GA, age at examination, sex, and AL, residual clinical heterogeneity related to disease activity, recurrence pattern, treatment timing, and cumulative treatment exposure could not be fully excluded. In addition, ROP zone and stage were not assigned to the spontaneously R-ROP group after stabilization because these classifications describe active disease severity and may vary during the disease course. This limited direct comparison of active-phase disease severity between spontaneously regressed and treated ROP eyes. Third, the treatment groups were imbalanced, and LP + IVI clinical-background group remained relatively small compared with the LP group. Fourth, functional assessment was limited primarily to BCVA; more sensitive measures such as microperimetry, contrast sensitivity, electroretinography, or fixation stability were not available. Fifth, AO-SLO imaging in children requires adequate fixation and image quality, which may introduce selection bias toward more cooperative children or less severe phenotypes.[36−39] In addition, AO-SLO image scaling was not corrected using individualized AL-based ocular magnification correction, although AL was included as a covariate in the multivariable models. Finally, several secondary and correlation analyses were exploratory and should be interpreted in the context of multiple comparisons.

In conclusion, AO-SLO identified selective temporal cone photoreceptor mosaic alterations in children with ROP, characterized by altered cone spatial organization rather than uniform photoreceptor loss. These cross-sectional findings extend prior AO observations to a larger pediatric cohort and support AO-SLO as a complementary imaging modality for evaluating photoreceptor mosaic organization in ROP survivors. Future longitudinal studies incorporating broader functional assessments are needed to clarify the clinical significance of these findings.

Acknowledgments

The authors would like to thank all members of our research team for their valuable support and collaboration throughout this project.

Footnotes and Disclosures

Originally received: June 10, 2026.
Final revision: August 25, 2026.
Accepted: September 9, 2026.
Available online: September 21, 2026.Manuscript no. XOPS-D-26-00679.

[1] Shenzhen Eye Hospital, Jinan University, Shenzhen Eye Institute, Shenzhen, China.

[2] Center for Preventative Ophthalmology and Biostatistics, Department of Ophthalmology, Perelman School of Medicine, University of Pennsylvania, Philadelphia, Pennsylvania.

[†]Y.L., J.T., and X.Z. contributed equally to this work and share first authorship.

Disclosure(s):

The Article Publishing Charge (APC) for this article was paid by Shenzhen Eye Hospital using research grant funds.

All authors have completed and submitted the ICMJE disclosures form.

The authors have no proprietary or commercial interest in any materials discussed in this article.

Data Availability: The data sets generated and/or analyzed during the current study are not publicly available due to participant privacy but are available from the first author on reasonable request.

This study was supported by the National Natural Science Foundation of China (82271103, 82671377); the Shenzhen Medical Research Fund (C2301005, C2501034, D250403004); the Shenzhen Science and Technology Program (ZDYJ20251211141301002); the Sanming Project of Medicine in Shenzhen (SZSM202311018); and the China Postdoctoral Science Foundation (2026M792291).

HUMAN SUBJECTS:

Human subjects were included in this study. This cohort study conducted at Shenzhen Eye Hospital was approved by the Institutional Review Board of Shenzhen Eye Hospital (Shenzhen, China; approval number: 20191206-01) and was conducted in accordance with the tenets of the Declaration of Helsinki. Written informed consent was obtained from the legal guardians of each participating child.

No animal subjects were used in this study.

Author Contributions:

Conception and design: Liu, Tang, Ying

Analysis and interpretation: Liu, Tang, Ying

Data collection: Liu, Tang, Zhao, Hu, Zhou, Yu, Luo, Zheng

Obtained funding: Liu, Zhang

Overall responsibility: Liu, Tang, Ying, Zhang. Obtained funding: Liu, Zhang

Abbreviations and Acronyms:

AL = axial length; **AO** = adaptive optics; **AO-SLO** = adaptive optics scanning laser ophthalmoscopy; **BCVA** = best-corrected visual acuity; **GA** = gestational age; **GEE** = generalized estimating equation; **IRT** = inner retinal thickness; **IVI** = intravitreal injection; **LP** = laser photocoagulation; **ORT** = outer retinal thickness; **P-noROP** = preterm without ROP; **ROP** = retinopathy of prematurity; **R-ROP** = regressed ROP; **SS-OCT** = swept-source OCT.

Keywords:

Retinopathy of prematurity, Adaptive optics scanning laser ophthalmoscopy, Cone photoreceptor, Cone mosaic alterations, Retinal imaging.

Correspondence:

Guoming Zhang, PhD, Shenzhen Eye Hospital, Jinan University, Shenzhen Eye Institute, Shenzhen 518040, China. E-mail: zhangguoming@sz-eyes.com; and Guishuang Ying, PhD, 3711 Market Street, Suite 801, Philadelphia, PA 19104. E-mail: gsying@pennmedicine.upenn.edu.

References

1. Blencowe H, Lawn JE, Vazquez T, et al. Preterm-associated visual impairment and estimates of retinopathy of prematurity at regional and global levels for 2010. *Pediatr Res*. 2013;74 Suppl 1(Suppl 1):35−49.
2. Chen J, Zhu Y, Li L, et al. Visual impairment burden in retinopathy of prematurity: trends, inequalities, and improvement gaps. *Eur J Pediatr*. 2024;183(4):1891−1900.
3. Akula JD, Arellano IA, Swanson EA, et al. The fovea in retinopathy of prematurity. *Invest Ophthalmol Vis Sci*. 2020;61(11):28.
4. Lepore D, Quinn GE, Molle F, et al. Follow-up to age 4 years of treatment of type 1 retinopathy of prematurity intravitreal Bevacizumab injection versus laser: fluorescein angiographic findings. *Ophthalmology*. 2018;125(2):218−226.
5. Balasubramanian S, Beckmann J, Mehta H, et al. Relationship between retinal thickness profiles and visual outcomes in young adults born extremely preterm: the EPICure@19 Study. *Ophthalmology*. 2019;126(1):107−112.
6. Maldonado RS, O'Connell RV, Sarin N, et al. Dynamics of human foveal development after premature birth. *Ophthalmology*. 2011;118(12):2315−2325.
7. Chavala SH, Farsiu S, Maldonado R, et al. Insights into advanced retinopathy of prematurity using handheld spectral domain optical coherence tomography imaging. *Ophthalmology*. 2009;116(12):2448−2456.
8. Ooto S, Hangai M, Takayama K, et al. High-resolution imaging of the photoreceptor layer in epiretinal membrane using adaptive optics scanning laser ophthalmoscopy. *Ophthalmology*. 2011;118(5):873−881.
9. Williams DR, Burns SA, Miller DT, Roorda A. Evolution of adaptive optics retinal imaging [Invited]. *Biomed Opt Express*. 2023;14(3):1307−1338.
10. Makiyama Y, Ooto S, Hangai M, et al. Macular cone abnormalities in retinitis pigmentosa with preserved central vision using adaptive optics scanning laser ophthalmoscopy. *PLoS One*. 2013;8(11):e79447.
11. Ooto S, Hangai M, Sakamoto A, et al. High-resolution imaging of resolved central serous chorioretinopathy using adaptive optics scanning laser ophthalmoscopy. *Ophthalmology*. 2010;117(9):1800−1809.
12. Fang D, Liang J, Diao Y, et al. Morphologic and functional assessment of photoreceptors in laser-induced retinopathy using adaptive optics scanning laser ophthalmoscopy and microperimetry. *Am J Ophthalmol*. 2024;265:61−72.
13. Wang X, Sadda SR, Ip MS, et al. In vivo longitudinal measurement of cone photoreceptor density in intermediate age-related macular degeneration. *Am J Ophthalmol*. 2023;248:60−75.
14. Ramamirtham R, Akula JD, Soni G, et al. Extrafoveal cone packing in eyes with a history of retinopathy of prematurity. *Invest Ophthalmol Vis Sci*. 2016;57(2):467−475.
15. Wells-Gray EM, Choi SS, Bries A, Doble N. Variation in rod and cone density from the fovea to the mid-periphery in healthy human retinas using adaptive optics scanning laser ophthalmoscopy. *Eye (Lond)*. 2016;30(8):1135−1143.
16. Li K, Yin Q, Ren J, et al. Automatic quantification of cone photoreceptors in adaptive optics scanning light ophthalmoscope images using multi-task learning. *Biomed Opt Express*. 2022;13(10):5187−5201.
17. Liang J, Zou Z, Chen L, et al. Cone structure and retinal sensitivity assessment in patients with red-green colour vision deficiency using multimodal imaging. *Br J Ophthalmol*; 2026. https://doi.org/10.1136/bjo-2025-329412.
18. F A. Voronoi diagrams: a survey of a fundamental geometric data structure. *ACM Comput Surv*. 1991;23(3):345−405.
19. Good WV. Retinopathy of prematurity incidence in children. *Ophthalmology*. 2020;127(4S):S82−S83.

20. Ingvaldsen SH, Morken TS, Austeng D, Dammann O. Visuopathy of prematurity: is retinopathy just the tip of the iceberg? *Pediatr Res*. 2022;91(5):1043–1048.
21. Yuodelis C, Hendrickson A. A qualitative and quantitative analysis of the human fovea during development. *Vis Res*. 1986;26(6):847–855.
22. Menghini M, Lujan BJ, Zayit-Soudry S, et al. Correlation of outer nuclear layer thickness with cone density values in patients with retinitis pigmentosa and healthy subjects. *Invest Ophthalmol Vis Sci*. 2014;56(1):372–381.
23. Ryan SJ, Hinton DR, Schachat AP, Wilkinson CP. Sadda. In: Wiedemann P, ed. *Retina*. 5th ed. Philadelphia, PA: Saunders Elsevier; 2013.
24. Dorrell MI, Aguilar E, Jacobson R, et al. Antioxidant or neurotrophic factor treatment preserves function in a mouse model of neovascularization-associated oxidative stress. *J Clin Invest*. 2009;119(3):611–623.
25. Levin LA, Nilsson SFE. Ver Hoeve. In: Wu SM, Kaufman PL, Alm A, eds. *Adler's Physiology of the Eye*. 5th ed. Edinburgh; New York: Saunders/Elsevier; 2011.
26. Kurihara T, Westenskow PD, Bravo S, et al. Targeted deletion of Vegfa in adult mice induces vision loss. *J Clin Invest*. 2012;122(11):4213–4217.
27. Geloneck MM, Chuang AZ, Clark WL, et al. Refractive outcomes following bevacizumab monotherapy compared with conventional laser treatment: a randomized clinical trial. *JAMA Ophthalmol*. 2014;132(11):1327–1333.
28. Lu X, Zeng X, Chen M, et al. Refractive and biometrical characteristics of children with retinopathy of prematurity who received laser photocoagulation or intravitreal ranibizumab injection. *Graefes Arch Clin Exp Ophthalmol*. 2022;260(10):3213–3219.
29. Marlow N, Stahl A, Lepore D, et al. 2-year outcomes of ranibizumab versus laser therapy for the treatment of very low birthweight infants with retinopathy of prematurity (RAINBOW extension study): prospective follow-up of an open label, randomised controlled trial. *Lancet Child Adolesc Health*. 2021;5(10):698–707.
30. O'Connor AR, Stephenson T, Johnson A, et al. Long-term ophthalmic outcome of low birth weight children with and without retinopathy of prematurity. *Pediatrics*. 2002;109(1):12–18.
31. Zeng X, Chen M, Zheng L, et al. Study of the biological developmental characteristics of the eye in children after laser surgery for the treatment of retinopathy of prematurity. *Front Med (Lausanne)*. 2021;8:783552.
32. Wang Y, Bensaid N, Tiruveedhula P, Ma J, Ravikumar S, Roorda A. Human foveal cone photoreceptor topography and its dependence on eye length. *eLife*. 2019;8:e47148.
33. Liang J, Fang D, Diao Y, et al. Photoreceptor cone loss is associated with decreased deep retinal vessel density and impaired retinal sensitivity in high myopia. *Br J Ophthalmol*. 2025;109(10):1194–1200.
34. Munro RJ, Fulton AB, Chui TY, et al. Eye growth in term- and preterm-born eyes modeled from magnetic resonance images. *Invest Ophthalmol Vis Sci*. 2015;56(5):3121–3131.
35. Zhou WD, Dong L, Shi HX, et al. Cone mosaic in eyes with varied axial length using adaptive optics scanning laser ophthalmoscopy. *Photodiagnosis Photodyn Ther*. 2025;52:104517.
36. Panorgias A, Zawadzki RJ, Capps AG, et al. Multimodal assessment of microscopic morphology and retinal function in patients with geographic atrophy. *Invest Ophthalmol Vis Sci*. 2013;54(6):4372–4384.
37. Quaggin SE. Turning a blind eye to anti-VEGF toxicities. *J Clin Invest*. 2012;122(11):3849–3851.
38. Vohnsen B. Directional sensitivity of the retina: a layered scattering model of outer-segment photoreceptor pigments. *Biomed Opt Express*. 2014;5(5):1569–1587.
39. Westheimer G. Directional sensitivity of the retina: 75 years of Stiles-Crawford effect. *Proc Biol Sci*. 2008;275(1653):2777–2786.